

**Gate-controlled proximity magnetoresistance
in $\text{In}_{1-x}\text{Ga}_x\text{As}/(\text{Ga,Fe})\text{Sb}$ bilayer heterostructures**

Kosuke Takiguchi¹, Kyosuke Okamura¹, Le Duc Anh^{1,2,3}, and Masaaki Tanaka^{1,4,5}

¹ *Department of Electrical Engineering and Information Systems, The University of
Tokyo, Bunkyo-ku, Tokyo 113-8656, Japan*

² *Institute of Engineering Innovation, The University of Tokyo, Bunkyo-ku, Tokyo 113-
8656, Japan.*

³ *PRESTO, Japan Science and Technology Agency, Kawaguchi, Saitama, 332-0012,
Japan*

⁴ *Centre for Spintronics Research Network (CSRN), The University of Tokyo, Bunkyo-
ku, Tokyo 113-8656, Japan.*

⁵ *Institute for Nano Quantum Information Electronics, The University of Tokyo, 4-6-1,
Komaba, Meguro-ku, Tokyo 153-8505 Japan.*

Abstract

The magnetic proximity effect (MPE), ferromagnetic coupling at the interface of magnetically dissimilar layers, attracts much attention as a promising pathway for introducing ferromagnetism into a high-mobility non-magnetic conducting channel. Recently, our group found giant proximity magnetoresistance (PMR), which is caused by MPE at an interface between a non-magnetic semiconductor InAs quantum well (QW) layer and a ferromagnetic semiconductor (Ga,Fe)Sb layer. The MPE in the non-magnetic semiconductor can be modulated by applying a gate voltage and controlling the penetration of the electron wavefunction in the InAs QW into the neighboring insulating ferromagnetic (Ga,Fe)Sb layer. However, optimal conditions to obtain strong MPE at the InAs/(Ga,Fe)Sb interface have not been clarified. In this paper, we systematically investigate the PMR properties of $\text{In}_{1-x}\text{Ga}_x\text{As}$ ($x = 0\%, 5\%, 7.5\%, \text{ and } 10\%$) / (Ga,Fe)Sb bilayer semiconductor heterostructures under a wide range of gate voltage. The inclusion of Ga alters the electronic structures of the InAs thin film, in particular changing the effective mass and the QW potential of electron carriers. Our experimental results and theoretical analysis of the PMR in these $\text{In}_{1-x}\text{Ga}_x\text{As}/(\text{Ga,Fe})\text{Sb}$ heterostructures show that the MPE depends not only on the degree of penetration of the electron wavefunction into (Ga,Fe)Sb but also on the electron density. These findings help us to unveil the microscopic mechanism of MPE in semiconductor-based non-magnetic/ferromagnetic heterojunctions.

I. Introduction

Introducing a ferromagnetic coupling into a high-mobility semiconducting channel can lead to new types of spintronics devices with non-volatile and reconfigurable functions. One straightforward method towards this goal is doping magnetic impurities into a non-magnetic semiconductor, which led to the creation of ferromagnetic semiconductors (FMSs), such as (III,TM)V where TM is a transition metal element (Mn, Fe). However, carrier transport in FMSs is subject to frequent scatterings by the magnetic impurities, thus the carrier mobility is very low ($\sim 1 - 10 \text{ cm}^2/\text{Vs}$). For electronic device applications, it is important to obtain large magnetic responses in non-magnetic channels with high carrier mobility, minimizing scatterings by magnetic impurities. Utilizing a magnetic proximity effect (MPE), which is a magnetic coupling at the magnetically dissimilar layers, is one of the most promising pathways for this purpose [1–7]. In particular, bilayer systems consisting of a nonmagnetic (NM) conductive channel and a ferromagnetic (FM) insulator hold a magnetic coupling via MPE at the interface. In addition, since these bilayer systems have only one FM layer, the device fabrication is much simpler than that in the conventional spin-valve structures which contain FM/NM/FM tri-layer and more complicated multilayer structures [8–11]. Therefore, the magnetotransport phenomena induced by MPE in the FM/NM bilayers have been actively studied in metallic systems in recent years [12–18]. However, at these metallic NM/FM interfaces, the magnetoresistance (MR) magnitude is too small ($< 0.1 - 1 \%$) for practical purposes, which is mainly due to the short-range nature of the magnetic coupling ($< 1 \text{ nm}$).

In contrast, *semiconductor-based* NM/FM bilayer systems can overcome the problem of the metallic counterparts because the higher coherency and smaller

concentration of carriers enhance the interfacial magnetic coupling range. In particular, when we prepare a NM semiconducting quantum well (QW) interfaced with an insulating FM layer, as shown in Fig. 1(a), even small penetration of two-dimensional carrier's wavefunction in the QW into the neighbouring FMS layer is enough to yield a strong MPE. This is because the two-dimensional carrier system feels the spin-carrier interactions occurring at the interface *as a whole*, due to their high coherency. Furthermore, the MPE can be modulated by an external gate voltage, which enhances the penetration by pushing the wavefunction towards the FM side. Therefore, the spin splitting energy induced by MPE can be controlled by external electrical means.

Recently, we demonstrated the abovementioned advantage of the semiconductor NM/FM bilayer systems using a NM InAs QW/ FM (Ga,Fe)Sb [19]. The InAs/(Ga,Fe)Sb bilayer heterostructures have distinct merits as follows: (i) (Ga,Fe)Sb is a *p*-type FMS with high Curie temperature over 300 K [20,21]. (ii) The lattice mismatch between InAs and (Ga,Fe)Sb is only of the order of 0.1%, which allows epitaxial growth of high-quality single-crystalline heterostructures. (iii) InAs/(Ga,Fe)Sb has a type-III band lineup, in which the bottom of the conduction band of InAs is lower than the top of the valence band of (Ga,Fe)Sb at the NM/FM interface. This leads to large penetration of the electron wavefunction of the InAs QW into the (Ga,Fe)Sb side. (iv) At low temperature (< 5 K), the resistivity of (Ga,Fe)Sb is two-orders of magnitude higher than that of the InAs QW, thus electron carriers mainly flow in the InAs QW. The strong MPE led to a discovery of a new proximity magnetoresistance (PMR), whose magnitude reaches 20% at 10 T, which is twenty-fold larger than that of metallic systems, and a large spontaneous spin-splitting energy (~ 3.8 meV) in the InAs QW. Moreover, we successfully enhanced the PMR by applying a gate voltage.

However, in order to fully control the properties of the InAs/(Ga,Fe)Sb heterostructures and to realize practical spintronic applications, it is essential to obtain deeper insights into the microscopic mechanism of the MPE. To quantitatively estimate the MPE and spontaneous spin splitting energy induced in the NM channel, which is practically important, there are four main parameters that can be controlled experimentally; the penetration P of the electron wavefunction of the NM QW channel into the FM side, the electron concentration n , the barrier height E_b , and the effective mass m^* of the electron carriers in the NM QW. These four parameters are closely correlated. As shown in Fig. 1(a), the wavefunction $\varphi(z)$ decays exponentially in the FM insulator; $\varphi(z) = |\varphi_0| \exp[-(z - z_0)/\lambda]$, where $|\varphi_0|$ is the amplitude of the wavefunction at the interface, z is the axis in the growth direction, and z_0 is the position at the interface of NM/FM. Then, the penetration P is given by $P = |\varphi_0|\lambda$. According to the WKB approximation for tunnelling phenomena, $\lambda \propto 1/\sqrt{E_b}$ and $|\varphi_0| \propto (m^*)^{-1/4}$. Thus, large E_b and/or m^* suppress P and consequently the MPE. Larger n also leads to heavier m^* due to the non-parabolicity of the InAs conduction band and suppresses the MPE [22,23]. On the other hand, an important question is whether larger n can induce stronger MPE or not via enhancement of the interfacial s - d exchange coupling between electron carriers and Fe spins in the FMS, a well-known effect in conventional carrier-induced FMSs [24]. Therefore, in order to obtain larger spin splitting energy ΔE via MPE, investigating how ΔE depends on these trade-off parameters is crucial for seeking the optimal conditions.

In this paper, we investigate the PMR phenomena in field-effect transistor (FET) structures of $\text{In}_{1-x}\text{Ga}_x\text{As}$ ($x = 0\%$, 5% , 7.5% , and 10%)/(Ga,Fe)Sb bilayers while applying a top gate voltage V_g . Compared with the previous study of PMR in InAs/(Ga,Fe)Sb [19], Ga inclusion in the InAs channel (InGaAs channel) changes the E_b and m^* , which affects

the penetration P . By the analysis of the PMR observed in these four samples, we find that ΔE depends on n and the momentum relaxation time τ of electron carriers. These results suggest that ΔE is almost proportional to n in an accumulation state of the FET operation, which indicates that the spin splitting via MPE is induced not only by the penetration P of the wavefunction but also by the large carrier density n .

II. Experiment

We grew heterostructures consisting of $\text{In}_{1-x}\text{Ga}_x\text{As}$ (15 nm, $x = 0\%$, 5%, 7.5%, 10%)/ $(\text{Ga,Fe})\text{Sb}$ (15 nm, Fe 20%)/ AlSb (140 nm)/ AlAs (10 nm)/ GaAs (100 nm) on semi-insulating GaAs (001) substrates by molecular beam epitaxy (MBE) (Fig. 1(b)). The growth temperature was 550 °C for the GaAs and AlAs layers, 470 °C for the AlSb layer, 250 °C for the $(\text{Ga,Fe})\text{Sb}$ layer and the $\text{In}_{1-x}\text{Ga}_x\text{As}$ layer. The Ga content ($= x$) was determined by the ratio of In and Ga fluxes, which were calibrated using reflection high-energy electron diffraction (RHEED) intensity oscillations. *In situ* RHEED patterns of the $\text{In}_{1-x}\text{Ga}_x\text{As}$ (Fig.1(c)-(f)) and $(\text{Ga,Fe})\text{Sb}$ (Fig.1(g)-(j)) layers were bright and streaky, indicating good crystal quality and smooth surface during the growth.

We first patterned the samples into 100 μm (width) \times 400 μm (length) Hall bars using standard photolithography and Ar ion milling, and then formed several electrodes (source S, drain D, and electrodes for transport measurements) using sputtering deposition and lift-off of an Au (50 nm)/Cr (5 nm) film. An insulating Al_2O_3 layer (~50 nm) was deposited as a gate insulator at 170 °C on the Hall bars using atomic layer deposition (ALD). It is known that depositing Al_2O_3 using ALD can decrease the interfacial state density at the $\text{In}_{1-x}\text{Ga}_x\text{As}/\text{oxide}$ interface [25,26]. Thus, it is expected that the modulation of the electrical properties by the gate voltage in our $\text{Al}_2\text{O}_3/\text{In}_{1-x}$

$x\text{Ga}_x\text{As}/(\text{Ga,Fe})\text{Sb}$ FETs is more effective than that of the $\text{HfO}_2/\text{InAs}/(\text{Ga,Fe})\text{Sb}$ FETs reported in our previous study of PMR [19]. Finally, we formed a top-gate electrode (G), again by sputtering deposition and lift-off processes of an Au (50 nm)/Cr (5 nm) film. Figure 1(k) shows an optical microscope image of the FET device examined in this study. We applied a gate voltage V_g between the G electrode and the S electrode. We measured the longitudinal resistance R_{xx} by a standard four-terminal method and the Hall resistance R_{xy} simultaneously at 2 K. In this study, a magnetic field B was always applied perpendicular to the film plane. In our recent study on the magnetotransport properties of $\text{InAs}/(\text{Ga,Fe})\text{Sb}$ bilayers, we have found a new type of odd-parity magnetoresistance (OMR), which is an odd function against B , and the resistance change reaches almost 13.5% of the total resistance at 10 T [27]. Although the OMR is also observed in this study, this phenomena is out of the scope of this paper and will be discussed elsewhere. Therefore, all the MR and the Hall resistance data in this work were obtained by extracting only the even- and odd-function components against B from the raw data, respectively. To obtain the QW potential and electron carrier wavefunctions in the $\text{In}_{1-x}\text{Ga}_x\text{As}$ channel, we performed a self-consistent calculation for the case of $x = 5\%$ using Nextnano3. We note that the Fermi level in this calculation was assumed to be pinned at 0.60 eV below the conduction band bottom of $(\text{Ga,Fe})\text{Sb}$ due to the Fe impurity band in the band gap of this FMS as estimated in our previous study [28].

III. RESULTS & DISCUSSIONS

Figure 2(a)-(d) show the MR data of $\text{In}_{1-x}\text{Ga}_x\text{As}$ ($x = 0\%$, 5% , 7.5% and 10%)/ $(\text{Ga,Fe})\text{Sb}$ FET devices, named as D_0 , D_5 , $D_{7.5}$, and D_{10} , respectively, with a wide range of V_g ($-10 \text{ V} < V_g < 10 \text{ V}$). As summarized in Fig. 3(a), the MRs at 1 T ($= [R_{xx}(B =$

1 T)– $R_{xx}(0\text{ T})/R_{xx}(0\text{ T})$) in D_0 , D_5 , and D_{10} show a systematic change from negative to positive when negative V_g is applied from 0 to -10 V . In $D_{7.5}$, the negative MR is suppressed to nearly zero at $V_g = -8\text{ V}$. This variation of PMR can be understood by contributions of both Kondo scattering and s - d exchange interaction at the NM/FM interface, as will be explained later. We fit a modified Khosla-Fischer model [19,29] using the following equations (eqs. (1) – (5)) to our experimental results shown in Fig. 2(a) – (d). We found that this model excellently describes the magnetotransport results in the non-magnetic $\text{In}_{1-x}\text{Ga}_x\text{As}$ channels with MPE.

$$\frac{\Delta\rho}{\rho} = -a^2 \ln(1 + b^2 H^2) + \frac{c^2 H^2}{1 + d^2 H^2}, \quad (1)$$

where

$$a = A_1 J D(E_F) [S(S + 1) + \langle M^2 \rangle], \quad (2)$$

$$b^2 = \left[1 + 4S^2 \pi^2 \left(\frac{2JD(E_F)}{g} \right)^4 \right] \left(\frac{g\mu_B}{\alpha k_B T} \right)^2, \quad (3)$$

$$c^2 = \frac{\sigma_1 \sigma_2 (\mu_1 + \mu_2)^2}{(\sigma_1 + \sigma_2)^2}, \quad (4)$$

$$d^2 = \frac{(\sigma_1 \mu_2 - \sigma_2 \mu_1)^2}{(\sigma_1 + \sigma_2)^2}. \quad (5)$$

In eq. (2) and (3), A_1 is a constant representing the contribution of spin scattering to the whole MR, α is a numerical factor that is on the order of unity, $D(E_F)$ is the density of states (DOS) at the Fermi level E_F , g is the effective Lande factor of the $\text{In}_{1-x}\text{Ga}_x\text{As}$ QW, $\langle M^2 \rangle$ is the averaged squared magnetization, S is the localized spin moment of (Ga,Fe)Sb (we assume $S = 5/2$ for Fe^{3+} ions in (Ga,Fe)Sb), and J is the s , p - d exchange interaction energy at the NM/FM bilayer interface. In eq. (4) and (5), σ_i and μ_i represent the conductivity and mobility of electron carriers in $\text{In}_{1-x}\text{Ga}_x\text{As}$, respectively. The subscripts

1 and 2 of each parameter denote the majority and minority spins, respectively. The first term on the right side of eq. (1), which gives a negative MR component is due to the Kondo scattering of electron carriers in the $\text{In}_{1-x}\text{Ga}_x\text{As}$ by the localized Fe spins at the (Ga,Fe)Sb interface. The second term on the right side of eq. (1), which gives a positive MR component, is caused by the s - d exchange interaction between transport carriers in $\text{In}_{1-x}\text{Ga}_x\text{As}$ and the localized Fe spins at the interface of $\text{In}_{1-x}\text{Ga}_x\text{As}/(\text{Ga,Fe})\text{Sb}$. The fitting results using eq.(1) are shown by black dashed curves in Fig. 2 (a)-(d), showing excellent agreement with the experimental MR curves at various V_g .

From the modified Khosla-Fischer model of eq. (1), the interesting behavior of the PMR in our samples can be understood as follows: The negative MR component, which is induced by the Kondo effect, is enhanced under large penetration P of the electron carrier wavefunction into the FMS (Ga,Fe)Sb, as we experimentally proved in the previous work [19]. Considering the FET operation with a two-dimensional electron gas channel in the $\text{In}_{1-x}\text{Ga}_x\text{As}$ QW, there are three different regimes of the PMR depending on the gate voltage V_g , as shown in Fig. 3(b)-(d): (i, accumulation regime) As shown in Fig. 3(b), when a positive or zero V_g is applied, the wavefunction is tilted towards the Al_2O_3 layer side and the penetration of the electron wavefunction into the (Ga,Fe)Sb side is small but not zero. Therefore, the PMR shows small negative MR. In this regime, the electron carrier concentration n is larger than other regimes. (ii, depletion regime) As shown in Fig. 3(c), when a small negative or zero V_g is applied, the carrier wavefunction in the $\text{In}_{1-x}\text{Ga}_x\text{As}$ QW is pushed towards the FM (Ga,Fe)Sb side, which leads to the larger negative MR. The electron carrier concentration n is smaller than that in (i). (iii, inversion regime) As shown in Fig. 3(d), when a large negative V_g is applied, the channel is eventually inverted and hole carriers are induced at the $\text{Al}_2\text{O}_3/\text{InAs}$

interface far from the FMS side. These hole carriers do not interact with the magnetic moments in the (Ga,Fe)Sb layer, and thus MPE is again suppressed. Also, our calculation suggests that there are holes accumulated in the (Ga,Fe)Sb layer near the InAs/(Ga,Fe)Sb interface, which may lead to non-linear magnetic field dependence in the Hall resistance (See Supplementary Material). As the regime goes close to (iii), the PMR should be decreased. Therefore, when the V_g becomes more negative to enhance the penetration, the electrons are fully depleted eventually at negative large V_g and there is no MPE at all. In other words, appropriate V_g should be chosen to obtain the largest spin splitting ΔE .

Next, we discuss the dependence of ΔE on n and τ ($= \mu_n m^*/e$, μ_n is electron mobility), the data of which are shown in Fig. 4(a) and (b), respectively. ΔE in a two-dimensional electron system is estimated from the modified Khosla-Fischer model [19,29]:

$$\Delta E = 2\pi\hbar^2 \frac{n}{\mu_n m^*} d = \frac{2\pi\hbar^2}{e} \frac{n}{\tau} d, \quad (6)$$

where d is the fitting parameter from eq. (5). n and μ_n are estimated from the ordinary Hall effect measurements (Detailed discussions on the Hall effect data and analyses on $\text{In}_{1-x}\text{Ga}_x\text{As}/(\text{Ga,Fe})\text{Sb}$ are described in Supplemental Material). Here m^* of $\text{In}_{1-x}\text{Ga}_x\text{As}$, m_{InGaAs}^* , is determined by a linear intrapolation between the effective mass of InAs (m_{InAs}) and GaAs (m_{GaAs}), taken from literature: $m_{\text{In}_{1-x}\text{Ga}_x\text{As}}^*(x, n) = m_{\text{InAs}/(\text{Ga,Fe})\text{Sb}} + x[m_{\text{GaAs}}(n) - m_{\text{InAs}}(n)]$ [22,30], where $m_{\text{InAs}/(\text{Ga,Fe})\text{Sb}}$ is obtained by our recent study of Shubnikov-de Haas (SdH) oscillations in InAs/(Ga,Fe)Sb [31]. We have recently found that $m_{\text{InAs}/(\text{Ga,Fe})\text{Sb}}$ does not strongly depend on n , which is different from that in a NM InAs QW. In a usual NM InAs, m^* increases with increasing n because of the non-parabolicity of the InAs conduction band. However, in the present case of InAs/(Ga,Fe)Sb bilayers,

when we apply a positive gate voltage V_g , n is increased (making m^* heavier) but P is decreased (making m^* lighter due to the smaller s - d exchange interaction at the NM/FM interface). Thus, it is reasonable that m^* only weakly depends on n as observed experimentally [31]. According to eq (6), this result suggests that n and τ significantly affect the spin splitting ΔE .

Figure 4(a) shows the n -dependence of ΔE in all the FET devices (D_0 , D_5 , $D_{7.5}$, and D_{10} ; solid circles), comparing with the previous result in InAs/(Ga,Fe)Sb (\tilde{D}_0 ; open circles) [19]. Note that \tilde{D}_0 has a same semiconductor heterostructure as D_0 , and we re-estimate ΔE of the previous study in \tilde{D}_0 [19] by taking into account the n -dependence of m^* . At first, we found that unlike device \tilde{D}_0 in the previous work, ΔE of device D_0 , D_5 , $D_{7.5}$, and D_{10} increases with increasing n . In two particular devices \tilde{D}_0 and D_0 , both contain only an InAs channel ($x = 0$), the $\Delta E - n$ relationship shows a U-shape curve, where ΔE first decreases at $n < 1 \times 10^{13} \text{ cm}^{-2}$ (in device \tilde{D}_0) but increases at higher $n > 2 \times 10^{13} \text{ cm}^{-2}$ (in device D_0) as n increases. These results clearly indicate a general trend that the MPE is enhanced at larger n when increasing n above a specific threshold value. This can be explained by two counteracting effects of the gate voltage V_g on the MPE in our FET devices; the electron wavefunction penetration (P)- and electron concentration (n)-induced effects. In the region with small n (corresponding to regime (ii) at negative V_g), P is large and the penetration-induced effect dominates the MPE. An increase of V_g towards positive side decreases P and thus suppresses MPE. At large positive V_g (corresponding to regime (i)), while the penetration P is minimized, a larger n enhances the s - d exchange interaction at the InAs/(Ga,Fe)Sb interface, as commonly observed in carrier-induced FMSs. Thus the carrier-induced effect becomes more prominent, leading to stronger MPE and a larger spin splitting at the large- n region. These results clarify the

important roles of both factors, the electron concentration n and the penetration P of the electron wavefunction, for increasing the MPE and ΔE .

We note that the $\Delta E - n$ relationships in devices D₀, D₅, D_{7.5}, and D₁₀ do not show the increase of ΔE in the low- n region whereas device \tilde{D}_0 shows the increase of ΔE in the low n region due to the P -induced MPE. Comparing with the case of device \tilde{D}_0 , all the FET channels in device D₀, D₅, D_{7.5}, and D₁₀ quickly reach the inversion regime (the abovementioned regime iii) at negative V_g , where holes are increased and parallel conduction occurs (see also Supplemental Material). The difference might originate from the weaker pinning effect of the Fermi level in the Al₂O₃/In_{1-x}Ga_xAs/(Ga,Fe)Sb FETs than that in the HfO₂/InAs/(Ga,Fe)Sb FETs in the previous work [19]. The Khosla-Fischer model is thus unable to be used to estimate ΔE in this low- n region in devices D₀, D₅, D_{7.5}, and D₁₀. Further studies are required to determine ΔE in the NM channel in the low- n region without using Hall resistance data. For example, observing the spin-split Fermi surface using SdH oscillations is a promising approach, which will be reported elsewhere [31].

Finally, we comment on the $\Delta E - \tau$ relationship shown in Fig. 4(b). Comparing all the data shown in Fig. 4(b), it is found that ΔE increases with decreasing τ . From the modified Khosla-Fischer model, larger penetration P of the carrier wavefunction of the NM channel into the (Ga,Fe)Sb side, which enhances ΔE , leads to the larger spin-dependent scattering for the carriers and results in smaller τ . Therefore, the negative correlation between ΔE and τ can be reasonably understood.

IV. CONCLUSION

In conclusion, we investigate the MPE in semiconductor NM/FM heterostructures

by characterizing the magnetotransport properties of $\text{In}_{1-x}\text{Ga}_x\text{As}/(\text{Ga,Fe})\text{Sb}$ heterostructures. We performed the systematic analysis of the MPE by measuring the gate-controlled PMR using standard FET operation. These results clearly indicate a general trend that the $\Delta E - n$ characteristics follow a U-shape, and the MPE is enhanced at larger n when increasing n above a specific threshold value. From the $\Delta E - n$ characteristics, there are two counteracting effects that affect the ΔE ; one is determined by the electron concentration which leads to carrier-induced s - d exchange interaction at the NM/FM interface, and the other is determined by the penetration depth of the electron wavefunction into the ferromagnetic side. Therefore, in order to obtain large MPE, to choose the appropriate carrier concentration is crucial. The data obtained in this study will play an important role to unveil the microscopic mechanism of MPE in semiconductor-based non-magnetic/ferromagnetic heterostructures.

ACKNOWLEDGEMENTS

This work was partly supported by Grants-in-Aid for Scientific Research (18H05345, 20H05650, 20K15163, 20H02196), the CREST (JPMJCR1777) and PRESTO (JPMJPR19LB) Programs of JST, and the Spintronics Research Network of Japan (Spin-RNJ). A part of this work was conducted at the Advanced Characterization Nanotechnology Platform of the University of Tokyo, supported by the “Nanotechnology Platform” of the Ministry of Education, Culture, Sports, Science and Technology (MEXT), Japan.

DATA AVAILABILITY

The data that support the findings of this study are available from the corresponding author upon reasonable request.

References

- [1] I. Žutić, A. Matos-Abiague, B. Scharf, H. Dery, and K. Belashchenko, *Mater. Today* **22**, 85 (2018).
- [2] P. Lazić, K. D. Belashchenko, and I. Žutić, *Phys. Rev. B* **93**, 241401 (2016).
- [3] I. Vobornik, U. Manju, J. Fujii, F. Borgatti, P. Torelli, D. Krizmancic, Y. S. Hor, R. J. Cava, and G. Panaccione, *Nano Lett.* **11**, 4079 (2011).
- [4] S. Sakai, S. Majumdar, Z. I. Popov, P. V. Avramov, S. Entani, Y. Hasegawa, Y. Yamada, H. Huhtinen, H. Naramoto, P. B. Sorokin, and Y. Yamauchi, *ACS Nano* **10**, 7532 (2016).
- [5] T. Chiba, S. Takahashi, and G. E. W. Bauer, *Phys. Rev. B* **95**, 094428 (2017).
- [6] R. Watanabe, R. Yoshimi, M. Kawamura, M. Mogi, A. Tsukazaki, X. Z. Yu, K. Nakajima, K. S. Takahashi, M. Kawasaki, and Y. Tokura, *Appl. Phys. Lett.* **115**, 102403 (2019).
- [7] J. Xu, S. Singh, J. Katoch, G. Wu, T. Zhu, I. Žutić, and R. K. Kawakami, *Nat. Commun.* **9**, 2869 (2018).
- [8] M. N. Baibich, J. M. Broto, A. Fert, F. N. Van Dau, F. Petroff, P. Eitenne, G. Creuzet, A. Friederich, and J. Chazelas, *Phys. Rev. Lett.* **61**, 2472 (1988).
- [9] G. Binasch, P. Grünberg, F. Saurenbach, and W. Zinn, *Phys. Rev. B* **39**, 4828 (1989).
- [10] S. Yuasa, T. Nagahama, A. Fukushima, Y. Suzuki, and K. Ando, *Nat. Mater.* **3**, 868 (2004).
- [11] S. S. P. Parkin, C. Kaiser, A. Panchula, P. M. Rice, B. Hughes, M. Samant, and S.-H. Yang, *Nat. Mater.* **3**, 862 (2004).
- [12] H. Nakayama, M. Althammer, Y. T. Chen, K. Uchida, Y. Kajiwara, D. Kikuchi, T. Ohtani, S. Geprägs, M. Opel, S. Takahashi, R. Gross, G. E. W. Bauer, S. T. B. Goennenwein, and E. Saitoh, *Phys. Rev. Lett.* **110**, 206601 (2013).
- [13] Y.-T. Chen, S. Takahashi, H. Nakayama, M. Althammer, S. T. B. Goennenwein, E. Saitoh, and G. E. W. Bauer, *Phys. Rev. B* **87**, 144411 (2013).
- [14] C. O. Avci, K. Garello, A. Ghosh, M. Gabureac, S. F. Alvarado, and P. Gambardella, *Nat. Phys.* **11**, 570 (2015).
- [15] S. S. L. Zhang and G. Vignale, *Phys. Rev. B* **94**, 140411(R) (2016).
- [16] K. Ganzhorn, J. Barker, R. Schlitz, B. A. Piot, K. Ollefs, F. Guillou, F. Wilhelm, A. Rogalev, M. Opel, M. Althammer, S. Geprägs, H. Huebl, R. Gross, G. E. W. Bauer, and S. T. B. Goennenwein, *Phys. Rev. B* **94**, 094401 (2016).
- [17] D. Hou, Z. Qiu, J. Barker, K. Sato, K. Yamamoto, S. Vélez, J. M. Gomez-Perez, L. E. Hueso, F. Casanova, and E. Saitoh, *Phys. Rev. Lett.* **118**, 147202 (2017).
- [18] S. Cho, S. C. Baek, K.-D. Lee, Y. Jo, and B.-G. Park, *Sci. Rep.* **5**, 14668 (2015).

- [19] K. Takiguchi, L. D. Anh, T. Chiba, T. Koyama, D. Chiba, and M. Tanaka, *Nat. Phys.* **15**, 1134 (2019).
- [20] N. T. Tu, P. N. Hai, L. D. Anh, and M. Tanaka, *Phys. Rev. B* **92**, 144403 (2015).
- [21] N. T. Tu, P. N. Hai, L. D. Anh, and M. Tanaka, *Appl. Phys. Lett.* **108**, 192401 (2016).
- [22] L. D. Zivanov and M. B. Zivanov *CAS (IEEE, 1995)*, pp. 103–106.
- [23] P. Nam Hai, L. D. Anh, and M. Tanaka, *Appl. Phys. Lett.* **101**, 252410 (2012).
- [24] T. Jungwirth, W. A. Atkinson, B. H. Lee, and A. H. MacDonald, *Phys. Rev. B* **59**, 9818 (1999).
- [25] H. Zhao, J. Huang, Y. T. Chen, J. H. Yum, Y. Wang, F. Zhou, F. Xue, and J. C. Lee, *Appl. Phys. Lett.* **95**, 253501 (2009).
- [26] R. Suzuki, N. Taoka, M. Yokoyama, S. H. Kim, T. Hoshii, T. Maeda, T. Yasuda, O. Ichikawa, N. Fukuhara, M. Hata, M. Takenaka, and S. Takagi, *J. Appl. Phys.* **112**, 084103 (2012).
- [27] K. Takiguchi, L. D. Anh, T. Chiba, R. Fukuzawa, T. Takahashi, and M. Tanaka, *arXiv 2003.11731* (2020).
- [28] K. Sriharsha, L. D. Anh, N. T. Tu, S. Goel, and M. Tanaka, *APL Mater.* **7**, 021105 (2019).
- [29] R. P. Khosla and J. R. Fischer, *Phys. Rev. B* **2**, 4084 (1970).
- [30] C. Gauer, J. Scriba, A. Wixforth, J. P. Kotthaus, C. R. Bolognesi, C. Nguyen, B. Brar, and H. Kroemer, *Semicond. Sci. Technol.* **9**, 1580 (1994).
- [31] K. Takiguchi, H. Shiratani, L. D. Anh, and M. Tanaka, (in preparation).

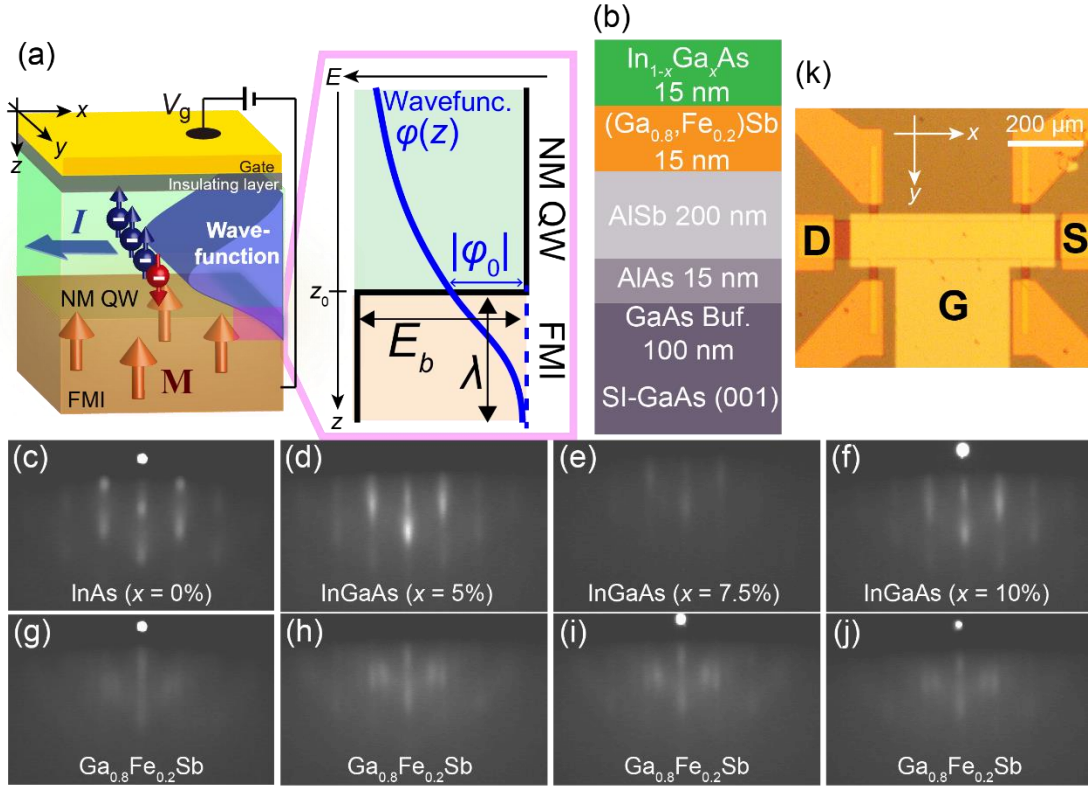


FIG. 1 (a) Schematic (left) device structure and (right) band alignment with electron carrier wavefunction (blue curve) in a NM QW/ FM insulator (FMI) heterostructure. In the left image, the wavefunction in the NM QW penetrates into the FMI. When an electrical current I flows in the in-plane direction, electrons interact with the neighboring magnetization \mathbf{M} at the interface, and are partially magnetized by MPE. A semiconductor-based NM/FM system enables modulation of the MPE by controlling the wavefunction with a top gate voltage V_g . In the right image, black solid line indicates the conduction band bottom of both materials. The carrier wavefunction penetrates into the FMI side with a penetration depth λ , determined by the barrier height E_b and the wavefunction amplitude at the interface $|\phi_0|$. (b) Sample structure of D0, D5, D7.5, and D10 with $x = 0\%$, 5%, 7.5% and 10%, respectively. (c)–(f) RHEED patterns of $\text{In}_{1-x}\text{Ga}_x\text{As}$ and (g)–(j) those of $(\text{Ga,Fe})\text{Sb}$ during the MBE growth of $\text{In}_{1-x}\text{Ga}_x\text{As}/(\text{Ga,Fe})\text{Sb}$ heterostructures with $x = 0\%$, 5%, 7.5% and 10%, respectively. (k) Top-view optical microscopy image of the FET device ($x = 5\%$, D5) examined in this study. We apply an electron current from the source (S) to the drain (D) and a gate voltage V_g from the gate electrode (G) to S.

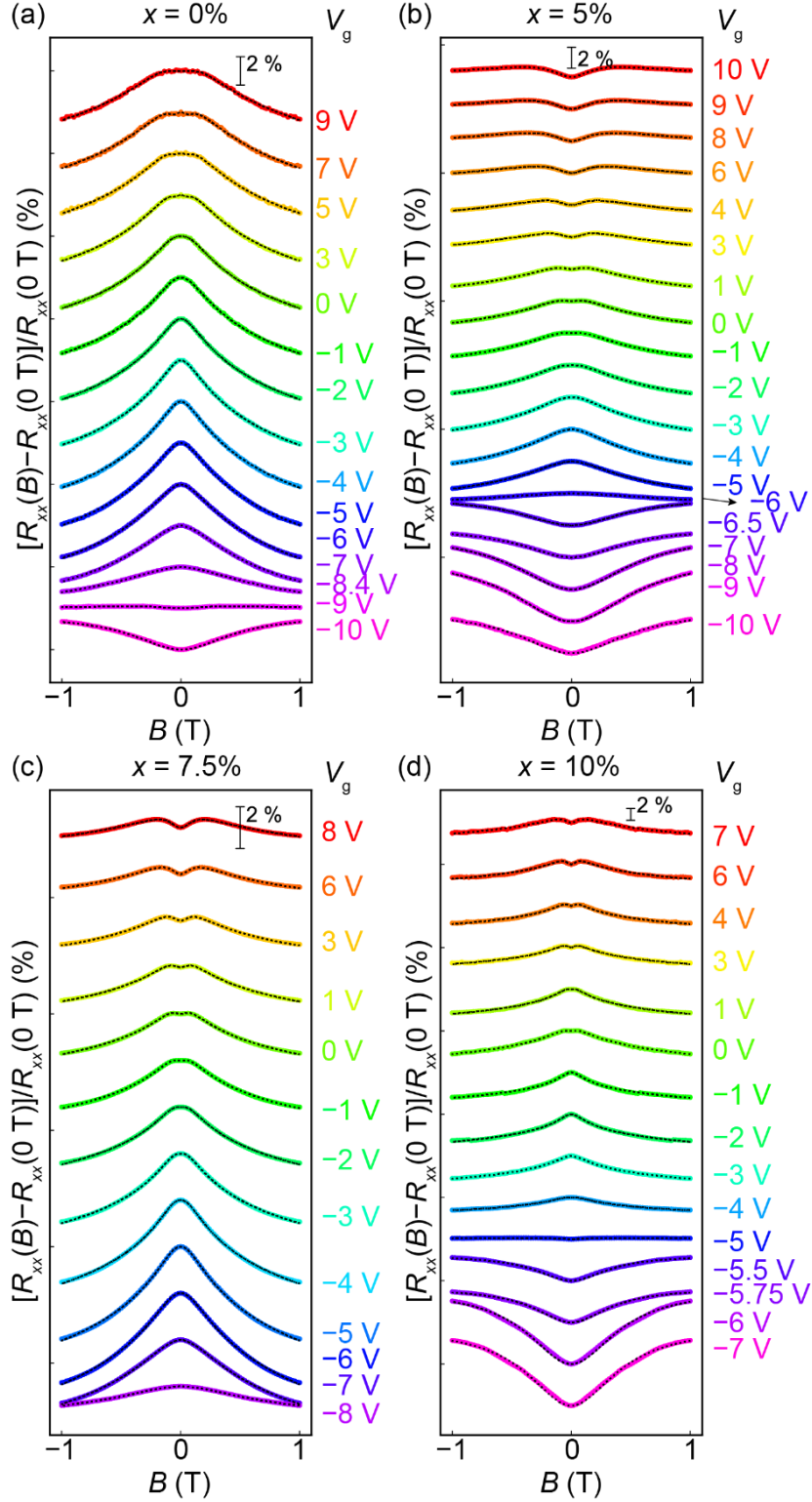


FIG. 2 (a)–(d) Magnetoresistance (MR) ($[R_{xx}(B) - R_{xx}(0 \text{ T})]/R_{xx}(0 \text{ T})$) of the $\text{In}_{1-x}\text{Ga}_x\text{As}/(\text{Ga,Fe})\text{Sb}$ heterostructures with $x = 0\%$, 5% , 7.5% and 10% under various V_g with a perpendicular magnetic field B (\parallel [001] of GaAs substrate) at 3.5 K , respectively. The black dashed curves represent the fitting results from eq. (1). The MR curves of $x = 0\%$, 5% , 7.5% and 10% at each V_g have been offset by 2.5% , 2.5% , 2% and 5% for a clearer view, respectively.

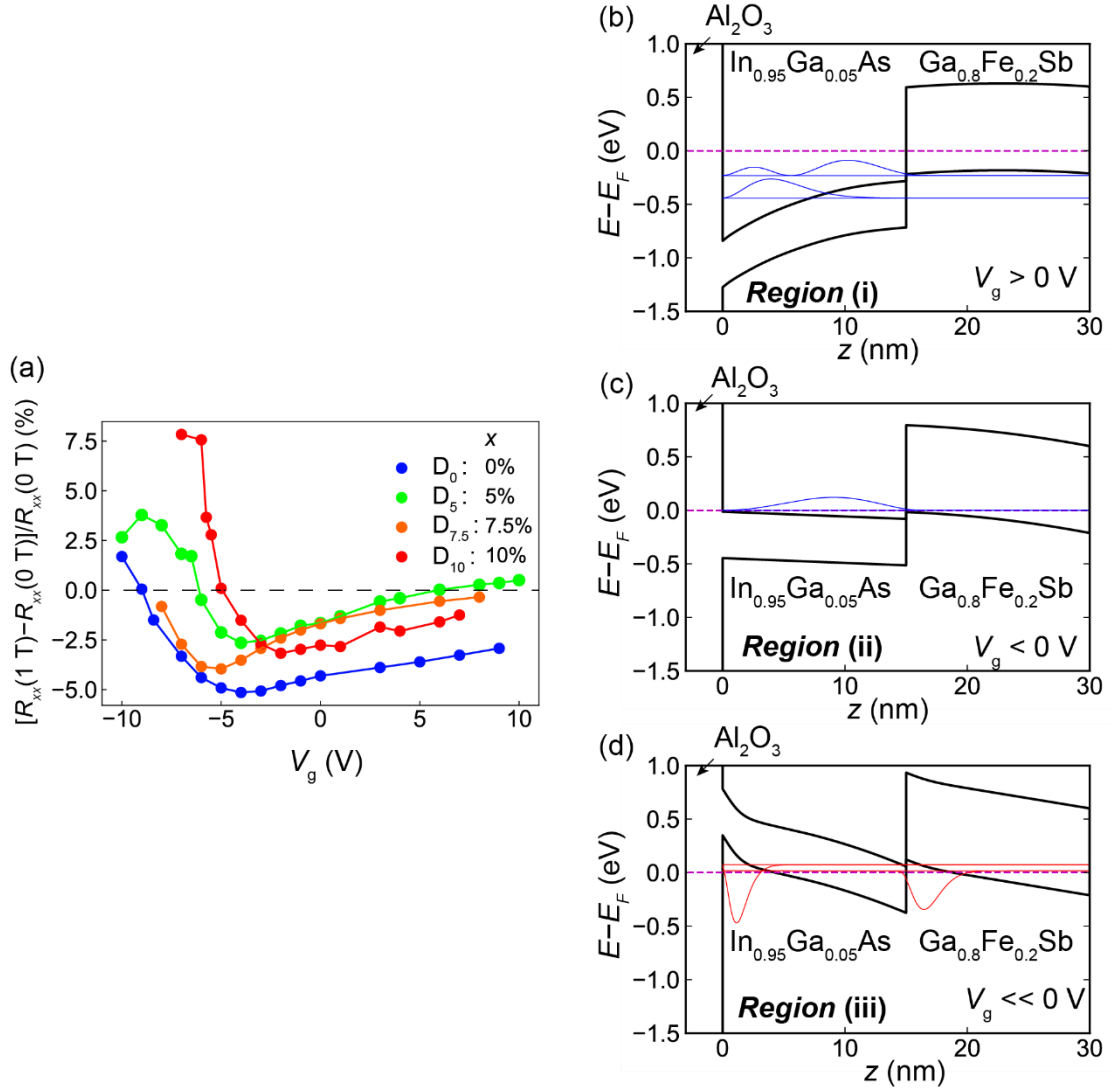


FIG. 3 V_g dependence of the MR ratio at 1 T ($= [R_{xx}(1\text{ T}) - R_{xx}(0\text{ T})]/R_{xx}(0\text{ T})$) in all devices examined in this work. Blue, green, orange, and red points indicate the data of device D_0 , D_5 , $D_{7.5}$, and D_{10} , respectively. (b)–(d) Self-consistent calculation results of the band profile in device D_5 ($x = 5\%$) in the growth direction ($// z$). The blue and red curves indicate the electron and hole wavefunctions in accumulation ((b) $V_g > 0$ V, region (i)), depletion ((c) $V_g < 0$ V, region (ii)), and inversion ((d) $V_g \ll 0$ V, region (iii)) operation, respectively. Purple dashed line indicates the Fermi level E_F .

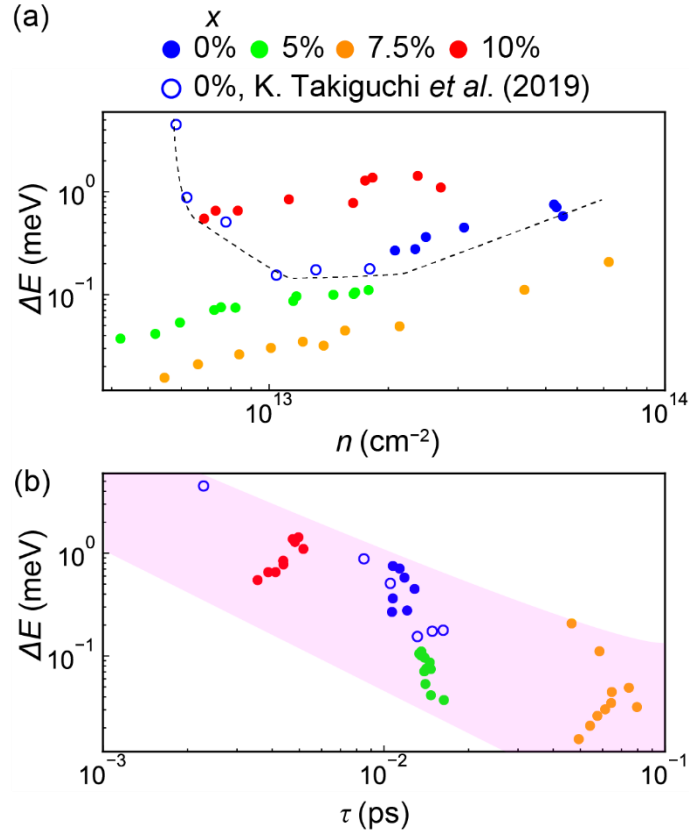


FIG. 4 (a) Spin splitting ΔE vs. electron concentration n and (b) relaxation time τ of device D_0 (blue), D_5 (green), $D_{7.5}$ (orange), and D_{10} (red). Blue open circles are for device \tilde{D}_0 [19]. Black dashed line in (a) is an eye-guide for a clear view of the InAs/(Ga,Fe)Sb data. The pink shaded area in (b) represents the eye-guide for the negative correlation of ΔE vs. τ .

Supplemental Material

Gate-controlled proximity magnetoresistance in $\text{In}_{1-x}\text{Ga}_x\text{As}/(\text{Ga,Fe})\text{Sb}$ bilayer heterostructures

Kosuke Takiguchi¹, Kyosuke Okamura¹, Le Duc Anh^{1,2,3}, & Massaaki Tanaka^{1,4,5}

¹ *Department of Electrical Engineering and Information Systems, The University of Tokyo, Bunkyo-ku, Tokyo 113-8656, Japan*

² *Institute of Engineering Innovation, The University of Tokyo, Bunkyo-ku, Tokyo 113-8656, Japan.*

³ *PRESTO, Japan Science and Technology Agency, Kawaguchi, Saitama, 332-0012, Japan*

⁴ *Centre for Spintronics Research Network, The University of Tokyo, Bunkyo-ku, Tokyo 113-8656, Japan.*

⁵ *Institute for Nano Quantum Information Electronics, The University of Tokyo, 4-6-1, Komaba, Meguro-ku, Tokyo 153-8505 Japan.*

Hall effect variation with gate voltage in $\text{In}_{1-x}\text{Ga}_x\text{As}/(\text{Ga,Fe})\text{Sb}$

As we discussed in the main manuscript, in order to estimate the spin-splitting energy ΔE from the PMR curve fitting, we need to measure the electron carrier concentration n and mobility μ_n . Figure S1(a)-(d) show the Hall measurement results of device D₀, D₅, D_{7.5}, and D₁₀, respectively. For the estimation of n and μ_n , we fit the B -linear component corresponding to the ordinary Hall effect (black dashed line) to the Hall resistance data in small negative $V_g \sim$ large positive V_g regions, shown by the yellow-colored regions in Fig. S1(a)-(d). In these regions, n monotonically decreases with decreasing V_g , which is consistent with the standard FET operation from regime (i) to (ii), as explained in the main manuscript.

On the other hand, the Hall resistances in all the devices show non-linear behavior especially in the large negative V_g regions, shown by the blue-colored regions in Fig. S1(a)-(d). In these regions, the non-linearity is too strong to be fit by the ordinary Hall effect. The non-linear Hall resistance curves in the $\text{In}_{1-x}\text{Ga}_x\text{As}/(\text{Ga,Fe})\text{Sb}$ bilayer heterostructures may be caused by two reasons, an anomalous Hall effect (AHE) and/or two-carrier conduction. In bilayer systems with MPE, it is reported that the Hall resistance shows the hysteresis curve corresponding to the magnetization of the FM layer even if the transport carriers mainly flow in the NM channel [1,2]. However, if this is the case, the Hall resistance vs. B curve should be proportional to the magnetization of the ferromagnetic (Ga,Fe)Sb layer. We do not observe any coercivity in the Hall measurements which corresponds to that of the (Ga,Fe)Sb magnetization. Thus, we consider that the non-linearity observed in our devices originates from the two-carrier conduction. We note that, as mentioned in the main manuscript, the modified Khosla-Fischer model is not applicable to the two-carrier regions. Thus, we do not present any

data of the spin splitting in Fig. 4.

In order to estimate the carrier density and mobility in two-carrier conduction region, we fit a two-carrier model [3] to the experimental Hall resistance R_{xy} – magnetic field B curves, as follows:

$$R_{xy} = \frac{p\mu_p^2 - n\mu_n^2 + (\mu_n\mu_p B)^2(p - n)}{e \left[(p\mu_p + n\mu_n)^2 + (\mu_n\mu_p B)^2(p - n)^2 \right]} B, \quad (\text{S1})$$

where $p(n)$, and $\mu_{p(n)}$ are the carrier concentration and mobility of holes (electrons), respectively. At various V_g , the fitting curves using eq. (S1) are shown by yellow solid curves in the blue-colored regions of Fig. S1 (a)-(d). Figure S2 shows the fitting results. In the large negative V_g region (blue region), there are extra holes with relatively larger μ_p than μ_n . There are two possible origins of this high-mobility holes: hole carriers in the InGaAs inversion layer and those in the valence band of (Ga,Fe)Sb. The holes in the InGaAs inversion layer is located far from the interface of (Ga,Fe)Sb as shown in Fig. 3(d), which do not interact via the s-d exchange coupling with the Fe spins in the FMS. Thus, they can possess high μ_p . Meanwhile, the holes in the coherent valence band of (Ga,Fe)Sb can also possess μ_p that is much higher than that ($< 10 \text{ cm}^2/\text{Vs}$) of the holes in the Fe-related impurity band [4] [5]. As shown in Fig. 3(d), these two kinds of holes can exist in the strong negative V_g region. We notice that, the trend of n and p against V_g does not match the standard FET operation corresponding to regime (iii). Since we do not have a clear answer for the carrier distribution and origin of holes, further study will be required.

References

- [1] S. Zhu, D. Meng, G. Liang, G. Shi, P. Zhao, P. Cheng, Y. Li, X. Zhai, Y. Lu, L. Chen, and K. Wu, *Nanoscale* **10**, 10041 (2018).
- [2] X. Liang, G. Shi, L. Deng, F. Huang, J. Qin, T. Tang, C. Wang, B. Peng, C. Song, and L. Bi, *Phys. Rev. Appl.* **10**, 024051 (2018).
- [3] R. A. Smith, *Semiconductors* (Cambridge University Press, Cambridge, 1978).
- [4] K. Sriharsha, L. D. Anh, N. T. Tu, S. Goel, and M. Tanaka, *APL Mater.* **7**, 021105 (2019).
- [5] T. Takeda, S. Sakamoto, K. Araki, Y. Fujisawa, L. D. Anh, N. Thanh Tu, Y. Takeda, S. Fujimori, A. Fujimori, M. Tanaka, and M. Kobayashi, *Phys. Rev. B* **102**, 245203 (2020).

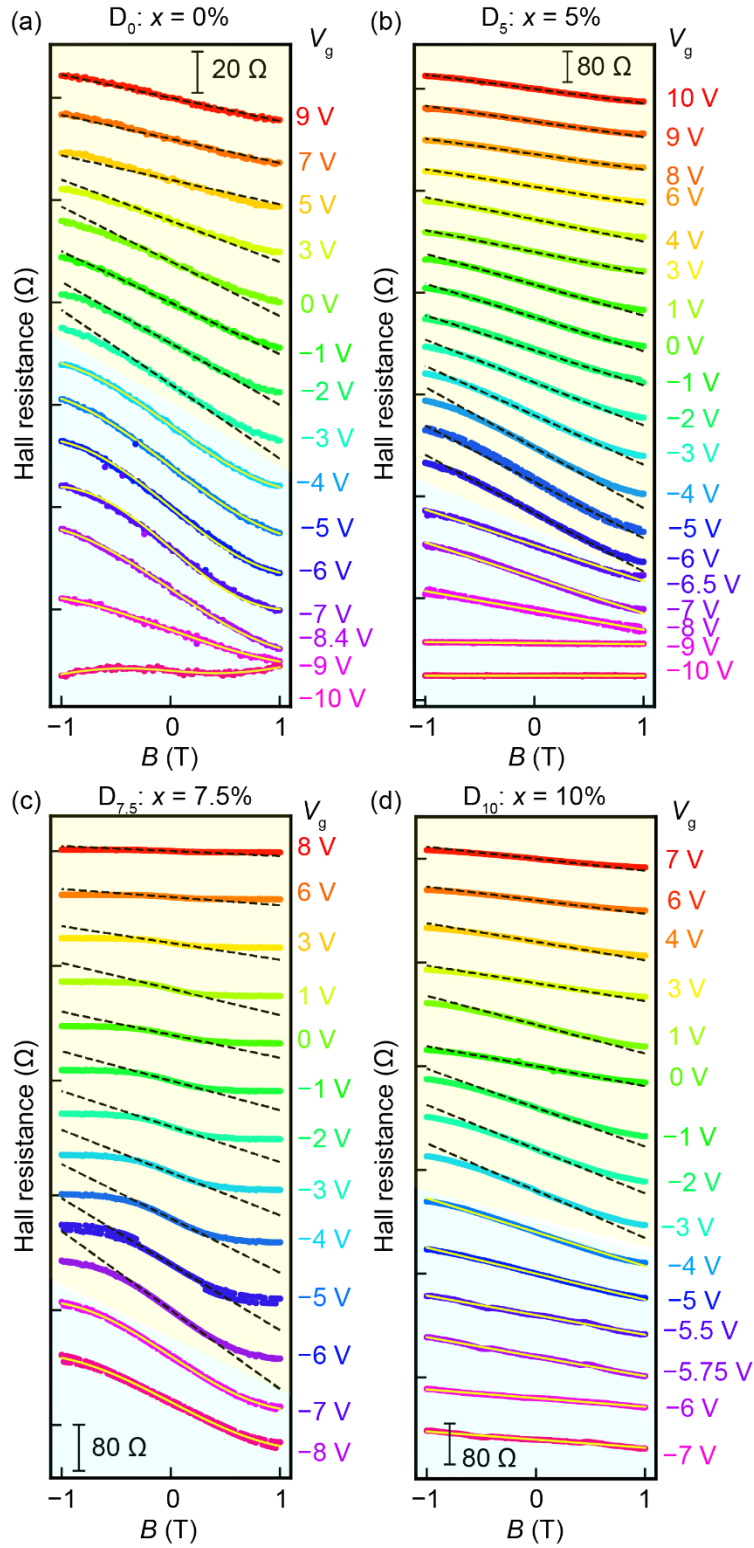


Figure S1 (a)-(d) Hall resistance curves of $x = 0\%$, 5% , 7.5% and 10% under various V_g with perpendicular magnetic field B (\parallel [001] of GaAs substrate) at 3.5 K, respectively. Black dashed lines in the yellow regions represent the fitting results of the ordinary Hall effect. Yellow solid curves in the blue regions represent the fitting results using eq. (S1). The Hall resistance curves at various V_g have been offset by 20Ω , 80Ω , 80Ω and 80Ω for easy viewing.

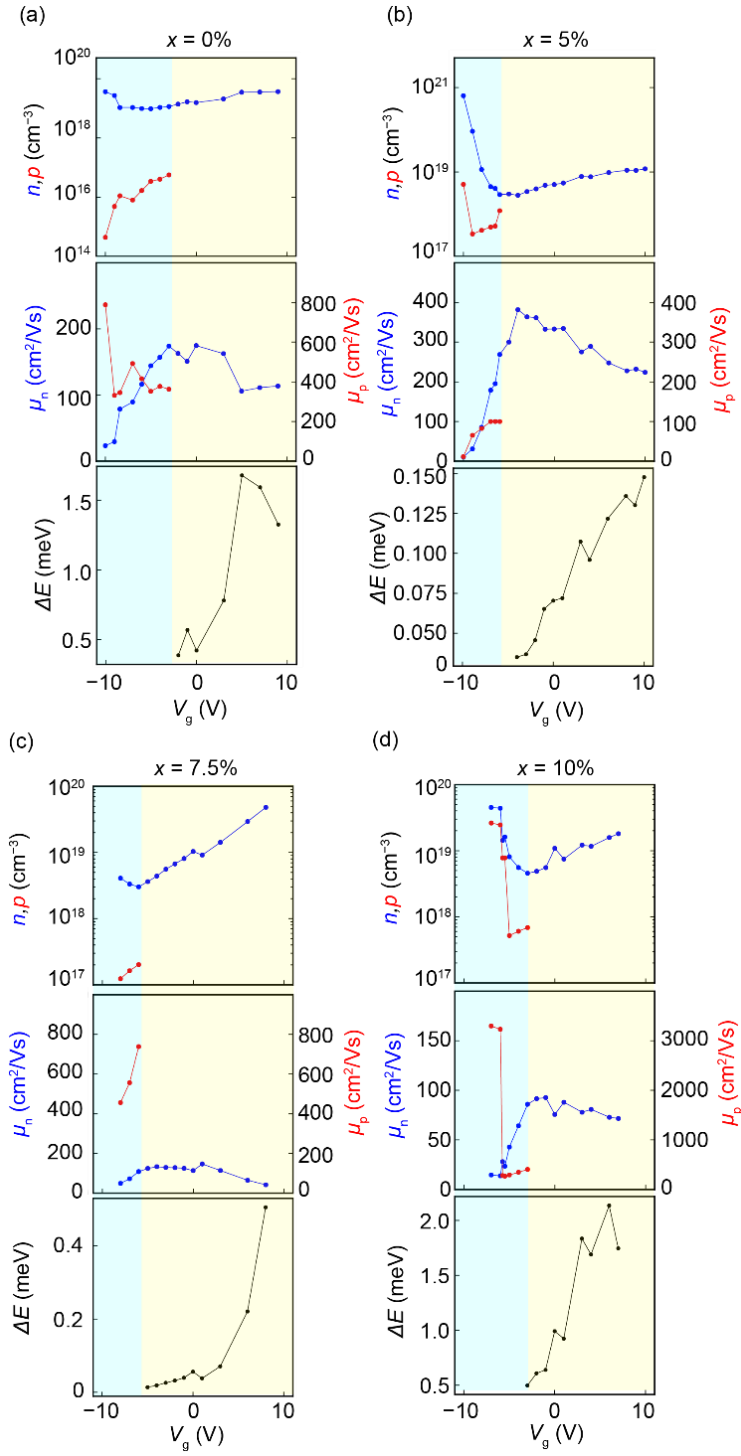


Figure S2 Fitting results of n , p , μ_n , μ_p , and ΔE , as a function of V_g with various x : (a) $x = 0\%$, (b) $x = 5\%$, (c) $x = 7.5\%$ and (d) $x = 10\%$, (upper panel) carrier concentration $n(p)$ and (middle panel) mobility $\mu_{n(p)}$ of electrons (holes) vs. V_g obtained by the fitting shown in Fig. S1. The blue and red points indicate electrons' and holes' parameters, respectively. (lower panel) Spin splitting ΔE vs. V_g . In the blue and yellow regions, the parameters are obtained by the two-carrier model and ordinary Hall effect, respectively. In the blue regions, ΔE cannot be measured since the modified Khosla-Fischer model is not applicable to the two-carrier conduction system.